KSME

Springer

Journal of Mechanical Science and Technology 34 (11) 2020

Original Article
DOI 10.1007/s12206-020-1031-5

Keywords:
· Hydroforming
· Metal thin-walled tube
· Plastic hardening
· Pulsating loading condition

Correspondence to:
Guolin Hu
379190074@qq.com

Citation:
Hu, G., Pan, C. (2020). Investigation of the plastic hardening of metal thin-walled tube under pulsating hydraulic loading condition. Journal of Mechanical Science and Technology 34 (11) (2020) 4743~4751.
http://doi.org/10.1007/s12206-020-1031-5

Received November 18th, 2019
Revised July 29th, 2020
Accepted August 28th, 2020

† Recommended by Editor Hyung Wook Park

Investigation of the plastic hardening of metal thin-walled tube under pulsating hydraulic loading condition

Guolin Hu and Chunrong Pan

School of Mechanical and Electrical Engineering, Jiangxi University of Science and Technology, 86 Hongqi Avenue, Zhanggong District, Ganzhou City, Jiangxi Province, China

Abstract In the present study, the mechanical model of section element in tube bulging area was established through the stress conditions of hydraulic bulging. Based on the mechanical model, the equivalent stress and equivalent strain equations of the section element in the bulging area were derived, respectively. Combined with the experimental data, the equivalent stress and strain of the section element in the bulging area were fitted by polynomial, and the plastic hardening model of thin-walled tube under pulsating loading was obtained. In order to verify the model precision, the plastic hardening models obtained from pulsating hydroforming and non-pulsating hydroforming were taken as the material model by finite element simulation respectively. The experimental results were compared with the simulation results which showed that as a pulsating hydraulic loading material parameters, the model established in this paper had higher precision.

1. Introduction

Tube pulsating hydraulic forming technology is a new research hotspot in recent years, which has been widely concerned by many researchers. It is expected to be a new technology to improve the forming properties of metal thin-walled tubes [1, 2]. The plastic hardening model, as a material property parameter, has a significant influence on the analysis of forming mechanism. Moreover, the accuracy of finite element simulation results is largely dependent on the accurate plastic hardening model. Some researchers obtain plastic hardening models based on simple loading paths using ordinary solution methods, such as unidirectional tensile and compression tests. Zhan et al. [3] investigated the forming mechanism of the welded tubes through a microhardness test. Badiger et al. [4-6] investigated the effect of cutting parameters on tool wear, cutting force and surface roughness in machining of MDN431 alloy. However, due to the different stress states between stretching and hydraulic bulging, the analysis accuracy of the plastic hardening model will be greatly reduced. Some researchers directly obtain the tube plastic hardening model by making assumptions about the tube bulging profile. Liu et al. [7] summarized the tube hydroforming process, and illustrated that the plastic hardening model can be obtained based on the assumption of the tube profile in the bulging process. Wang et al. [8] obtained the plastic hardening model by assuming that the shape of tube bulging profile was elliptic function under simple linear loading. Lin et al. [9] determined the flow stress equation of tube based on the experimental data of thin-walled tube in simple hydraulic bulging test. The above methods are all based on the assumption of the contour shape of the bulging area to obtain the relationship between stress and strain. Attentions were focused on the prediction error caused by the problem of both yield and flow cannot be reflected by the assumption that the yield equation is related to the plastic potential. Liu et al. [10] used a 3D digital speckle measuring system to obtain the deformation data of free tube bulging area online, and determined the plastic hardening model under simple linear loading. These methods require the use of curve fitting techniques, and the measurement methods of the tube axial curvature radius are complicated and costly, especially under complex loading conditions such as pulsating hydraulic

loading which has different loading history.

From what has been discussed above, it can be seen that most researchers have devoted to the law of plastic hardening in tube hydroforming under simple linear loading and have made some achievements. However, using the plastic hardening model under simple linear loading as the pulsating loading parameter will influence the accuracy of the numerical simulation. It is of great significance to find a tube plastic hardening model under complex loading conditions, such as pulsating hydraulic loading, which can enrich the model library of tube plastic hardening, and replacing the tube axial curvature radius measurement by strain measurement in the tube bulging area, which can provide a reference for more accurate analysis of the tube forming mechanism under pulsating hydraulic loading.

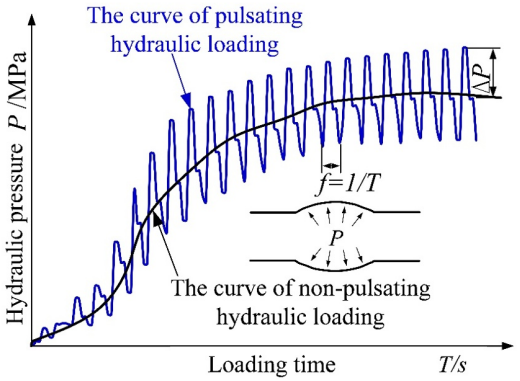

Fig. 1. Schematic diagram of tube hydroforming under pulsating hydraulic loading.

2. Plastic hardening of metal thin-walled tube under pulsating hydraulic loading

Tube pulsating hydraulic forming technology use a hydraulic pressure with pulsation frequency and amplitude acting on metal thin-walled tube internally to produce plastic deformation of the tube, as illustrated in Fig. 1. The plastic hardening model is used to describe the basic information of the tube deformation, which can accurately reflect the relationship between the stress and strain during the deformation process. The plastic constitutive models of metal materials are various, and common ones include power function models and polynomial models [11, 12]. The expression of the power function model is generally expressed as $\sigma = K\varepsilon^n$, which need to determine the parameters *K* and *n*. The expression of the polynomial model is generally expressed as $\sigma = \lambda_0 + \lambda_1\varepsilon^1 + \lambda_2\varepsilon^2 + ...$, which need to determine the coefficients before the polynomial.

The plastic hardening model has a significant influence on the analysis of tube forming mechanism, the evaluation of forming limit and the analysis of friction force between tube and die during tube forming. The research on plastic hardening model is mostly based on simple linear loading and the assumption of the tube profile in the bulging process, which is constructed on the basis of full amount theory. It is believed that the stress of material deformation is only related to the final strain state, and has nothing to do with the loading history [13]. However, the plastic increment theory is determined by the strain at each moment during the forming process, which can more accurately express the relationship between the stress and strain, especially for complex loading conditions such as pulsating loading [14].

2.1 The mechanical model of section element in tube bulging area

The construction of plastic hardening model for metal thin-walled tube is mainly to determine the relationship between stress and strain in the tube forming process. Therefore the mechanical model of the tube must be determined, and the calculation formulas of axial and circumferential stress should be obtained. The existing test equipment in this study can directly obtain the displacement field (three-dimensional point coordinates) of the bulging area at each forming. The curvilinear function of tube bulging profile can be obtained directly by test data fitting, and the tube axial curvature radius at each bulging can be determined.

The following assumptions were made before the establishment of the mechanical model of the tube and the relationship between the stress component and the deformation: (1) the volume of the tube remains unchanged during bulging process; (2) the tube material is isotropic; (3) in the tube bulging process, the end of tube can contract freely along the axis; (4) it is assumed that axial stress, circumferential stress and thickness stress are the main stresses of tube plastic deformation; (5) the influence of bending moment on tube deformation is ignored; (6) because the ratio of tube thickness to radius is very small (t_0/r_0 « 1), so the thickness stress is ignored.

Under the hydraulic pressure, the geometry of tube bulging area and the mechanical model of sectional element at any bulging moment are presented, as shown in Fig. 2.

According to the force analysis model of a unit body on the tube bulging profile (Fig. 2(b)), the axial direction force equation can be obtained, as shown in Eqs. (1)-(6):

$$\sigma_{z(i)} 2\pi t_i(\rho_{\theta(i)} - t_i/2)\cos\psi_i' = \pi P_i(\rho_{\theta(i)} - t_i)^2 - F_f \tag{1}$$

$$\sigma_{z(i)} = \frac{\pi P_i(\rho_{\theta(i)} - t_i)^2 - F_f}{2\pi t_i(\rho_{\theta(i)} - t_i/2)\cos\psi_i'} \tag{2}$$

$$F_f = \mu P_i 2\pi r_0 \frac{L-l}{2} \tag{3}$$

$$\psi_i' = \pi - \psi_i \tag{4}$$

$$\psi_i = \arctan f_{(z)}' \tag{5}$$

$$\rho_z = \left|\frac{[1 + f_{(z)}'^2]^{3/2}}{f_{(z)}''}\right| \tag{6}$$

where F_f is the friction force between the tube and the die, and the tube shrinkage during deformation is ignored when calculating the friction force. ψ_i is the angle between the tangent line

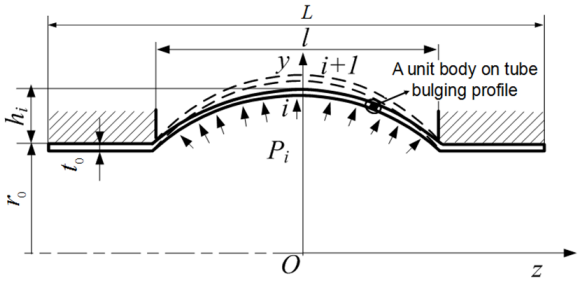

(a) Tube natural bulging model (half section)

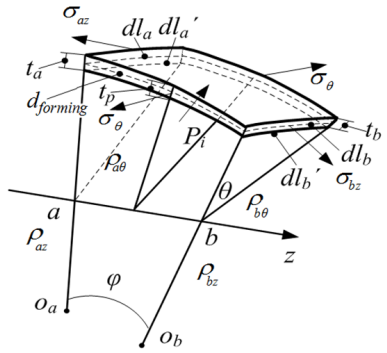

(b) The force condition of a unit body on tube bulging profile

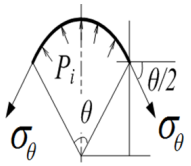

(c) The circumferential force condition of a unit body on tube bulging profile

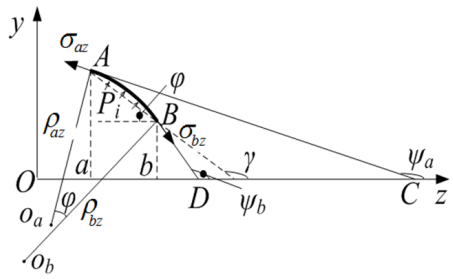

(d) The axial force condition of a unit body on tube bulging profile

Fig. 2. Mechanical model of a unit body on the tube bulging profile at any forming time.

at any point on the contour curve and the horizontal axis, and $f_{(z)}$ is the derivative of contour curve. According to the curvature Eq. (6), the curvature radius of each point on the axial contour curve of the tube of every bulging can be obtained.

According to the force analysis model of a unit body on the tube bulging profile (Fig. 2(d)), the equilibrium equation of the vertical direction force can be obtained, as shown in Eqs. (7)-(9):

$$\begin{aligned}&\sigma_{az}dl_a t_a \sin(\psi_a)+\sigma_{bz}dl_b t_b \sin(\psi_b)+2\sigma_\theta d_{forming}t_p \sin\frac{\theta}{2}\\&=P\frac{1}{2}(dl_a'+dl_b')d_{forming}\left|\cos\gamma\right|\end{aligned} \tag{7}$$

$$dl_a=(\rho_{a\theta}-t_a/2)\sin\theta \tag{8}$$

$$dl_b=(\rho_{b\theta}-t_b/2)\sin\theta. \tag{9}$$

Then the above parameters are substituted into the Eq. (7), the Eq. (10) can be obtained as follows:

$$\begin{aligned}&\sigma_{az}(\rho_{a\theta}-t_a/2)\sin\theta t_a\sin(\psi_a)\\&+\sigma_{bz}(\rho_{b\theta}-t_b/2)\sin\theta t_b\sin(\psi_b)+2\sigma_\theta d_{forming}t_p\sin\frac{\theta}{2}\\&=P\frac{1}{2}[(\rho_{a\theta}-t_a)+(\rho_{b\theta}-t_b)]\sin\theta d_{forming}\left|\cos\gamma\right|.\end{aligned} \tag{10}$$

As for tiny unit body, $\sin\theta=\theta$, $\sin\psi_a=\psi_a$, $\sin\psi_b=\psi_b$, then Eq. (10) can be transformed into Eq. (11):

$$\begin{aligned}&\sigma_{az}(\rho_{a\theta}-t_a/2)t_a\psi_a+\sigma_{bz}(\rho_{b\theta}-t_b/2)t_b\psi_b+\sigma_\theta d_{forming}t_p\\&=P\frac{1}{2}[(\rho_{a\theta}-t_a)+(\rho_{b\theta}-t_b)]d_{forming}\left|\cos\gamma\right|.\end{aligned} \tag{11}$$

By calculating ψ_a and ψ_b, then the circumferential stress can be obtained based on Eqs. (12) and (13):

$$t_p=(t_a+t_b)/2 \tag{12}$$

$$d_{forming}=\int_a^b\sqrt{1+[f'(z)]^2}dz. \tag{13}$$

Therefore, the circumferential stress of a unit body on the tube bulging profile was calculated, as shown in Eq. (14):

$$\sigma_\theta=\frac{\left\{\begin{array}{l}P[(\rho_{a\theta}-t_a)+(\rho_{b\theta}-t_b)]/2.\int_a^b\sqrt{1+f'(z)^2}dz.\left|\cos[(\psi_a+\psi_b)/2]\right|\\-[\sigma_{az}.(\rho_{a\theta}-t_a/2).t_a.\psi_a+\sigma_{bz}.(\rho_{b\theta}-t_b/2).t_b.\psi_b]\end{array}\right\}}{\int_a^b\sqrt{1+f'(z)^2}dz.(t_a+t_b)/2}. \tag{14}$$

When the tiny unit body is taken to the highest point of the bulged tube, it can be concluded that the shape of axial and circumferential contour at this point is an arc, and then Eqs. (15)-(19) below can be obtained:

$$\rho_{az}=\rho_{bz} \tag{15}$$

$$\rho_{a\theta}=\rho_{b\theta} \tag{16}$$

$$t_a=t_b=t_p \tag{17}$$

$$dl_a=dl_b=dl \tag{18}$$

$$\psi_i=\varphi/2\approx 0. \tag{19}$$

If the influence of friction force F_f at the end of the tube during the forming process is not considered, the axial stress and circumferential stress can be obtained, as shown in Eqs. (20) and (21):

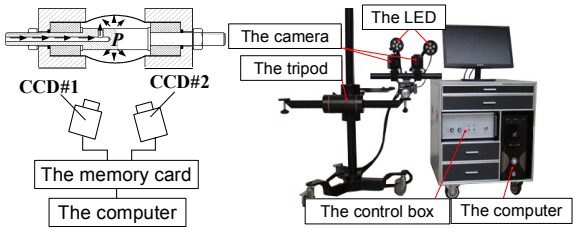

(a) The schematic diagram (b) The real figure

Fig. 3. High-speed 3D deformation and motion track detection system.

$$\sigma_z = \frac{P(\rho_\theta - t_p)^2}{2t_p(\rho_\theta - t_p/2)} \tag{20}$$

$$\sigma_\theta = \frac{P(\rho_\theta - t_p/2)}{t_p}[(1-\frac{t_p}{2(\rho_z - t_p/2)}) (1-\frac{t_p}{2(\rho_\theta - t_\theta/2)}) - \frac{(\rho_\theta - t_p)^2}{2(\rho_\theta - t_p/2)(\rho_z - t_p/2)}]. \tag{21}$$

2.2 The determination of equivalent strain of section element in tube bulging area

Due to the existing test equipment, the high speed 3D deformation and motion track detection and analysis system can obtain the axial strain and circumferential strain in the bulging area every time, the test equipment is illustrated in Fig. 3.

When the tube was in the hydraulically bulging process, the camera was used to aim at the tube bulging area, and the deformation process image of the tube bulging area was acquired in real time. The images are transmitted to the computer by the system of image memory card. The core technology of the analysis system is based on the digital image correlation technology and binocular stereo vision technology. By setting seed points, the characteristic image of the deformation body surface can be tracked to measure the three-dimensional coordinates, displacement and strain of the object during the deformation process. The obtained deformation images are processed by the system software installed on the computer to obtain dynamic deformation data such as three-dimensional displacement field, strain field and wall thickness reduction in the tube bulging area.

According to the law of constant volume of plastic deformation, the thickness strain of each tube bulging at all times can be obtained. And then the 3D strain increment of each tube bulging can be obtained, as shown in Eqs. (22) and (23):

$$\varepsilon_{\theta(i)} + \varepsilon_{z(i)} + \varepsilon_{t(i)} = 0 \tag{22}$$

$$\begin{aligned} d\varepsilon_{\theta(i)} &= \varepsilon_{\theta(i)} - \varepsilon_{\theta(i-1)} \\ d\varepsilon_{z(i)} &= \varepsilon_{z(i)} - \varepsilon_{z(i-1)} \\ d\varepsilon_{t(i)} &= \varepsilon_{t(i)} - \varepsilon_{t(i-1)}. \end{aligned} \tag{23}$$

According to the plastic increment theory, the equivalent strain increment in tube hydraulic bulging can be derived, as shown in Eqs. (24) and (25):

$$d\varepsilon_{e(i)} = \frac{\sqrt{2}}{3}\sqrt{(d\varepsilon_{\theta(i)} - d\varepsilon_{z(i)})^2 + (d\varepsilon_{z(i)} - d\varepsilon_{t(i)})^2 + (d\varepsilon_{t(i)} - d\varepsilon_{\theta(i)})^2} \tag{24}$$

$$\varepsilon_{e(i)} = \sum_{i=1}^{m}(d\varepsilon_{e(i)}). \tag{25}$$

2.3 The determination of equivalent stress of section element in tube bulging area

Equivalent stress is used to represent the comprehensive action of stress partial tensor in a point stress state during the deformation of an object. In general, in the process of mechanical analysis of the deformed body, the three stress components of the deformed body in the analysis process are equivalent to one stress, which is equivalent stress, to study the stress of the deformed body. Equivalent stress is also used to reflect the change of stress in the process of plastic deformation in the construction of plastic hardening model of metal thin-walled tube.

According to the plastic deformation work principle, in case the tube thickness stress is zero, the calculation of equivalent stress can be obtained, as shown in Eq. (26):

$$\sigma_{e(i)} = (\sigma_{\theta(i)} d\varepsilon_{\theta(i)} + \sigma_{z(i)} d\varepsilon_{z(i)}) / d\varepsilon_{e(i)}. \tag{26}$$

According to the previous analysis, when the strain increment of the tube in axial direction, circumferential direction, thickness direction and the equivalent strain increment of the corresponding time are obtained, the axial and circumferential stress can be calculated, and the equivalent strain and stress can be calculated.

The curve fitting technology of least square method is used to fit the calculated equivalent stress and equivalent strain, and the general polynomial form is directly used, as shown in Eq. (27):

$$\sigma_e = f(\varepsilon_e) = \lambda_0 + \lambda_1\varepsilon_e^1 + \lambda_2\varepsilon_e^2 + \lambda_3\varepsilon_e^3 + \ldots\ldots. \tag{27}$$

According to the above reasoning process, it is necessary to obtain the contour data to determine the curve function of the tube axial profile, and obtain the axial curvature radius of the tube bulging at each moment. In order to determine the equivalent strain of each point on the contour of tube bulging area, it is necessary to obtain the circumferential and axial strain of tube bulging in advance, and obtain the axial and circumferential strain increment of tube bulging in each forming.

2.4 Derivation of plastic hardening model of tube under pulsating hydraulic loading

It can be concluded from the theoretical analysis of plastic hardening model that if model parameters are to be quantified, the pulsating hydraulic bulging test of tube must be performed to measured data such as tube bulging instantaneous wall

Table 1. Geometrical parameters and material property parameters of the tube SS304.

Geometrical parameter	Value	Material property parameters	Value
t_0 / mm	0.6	σ_b / MPa	620
r_0 / mm	16	σ_s / MPa	310
L / mm	110	K/ MPa	1349.2
l / mm	50	n/ -	0.2879

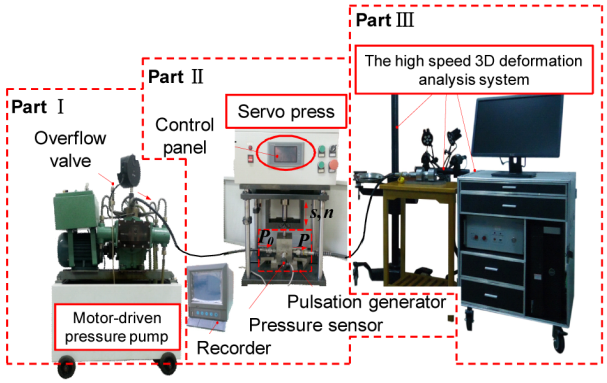

Fig. 4. Tube pulsating hydraulic bulging test system.

thickness of each moment, axial strain increment, circumferential strain increment, maximum radius of bulging processes and hydraulic pressure, etc. The tube pulsating hydraulic bulging test system is illustrated in Fig. 4.

The tube pulsating hydraulic bulging test system has three parts. Part I is the hydraulic system, which is used to generate hydraulic pressure; the part II is the pulsating system, which produces pulses of different frequencies and amplitudes; and the part III is the strain measuring system, which can obtain the axial and circumferential strain in the bulging area in each bulging process. The geometrical parameters and material property parameters of the thin-walled metal tube SS304 used in the test are shown in Table 1. The pulsating hydraulic loading curve used in the test is the same as Fig. 1. The loading curve can be expressed as $P = \Delta P \sin(2\pi ft) + P_0$, which the ΔP is the amplitude of pulsating fluid pressure fluctuation, and P_0 is the base fluid pressure. The amplitude of hydraulic pressure is determined according to the average value of fluctuation in the pulsating hydraulic loading curve. By setting the stamping stroke and motor speed of the servo stamping machine, and combining them to obtain different amplitudes and frequencies. The pulsating hydraulic loading curve can recorded online by pressure sensor, and the parameters of the pulsating hydraulic system used in the test are shown in Table 2. After the test, the tube wall thickness, the axial and circumferential curvature radius, the axial and circumferential strain can be obtained get through the tube pulsating hydraulic bulging test system.

Subsequently, the Eqs. (26) and (27) are used, respectively, to calculate the tube equivalent stress and equivalent strain value. And then, the least squares curve fitting technology is adopted to obtain the plastic hardening curve.

Table 2. The parameters of the pulsating hydraulic system.

ΔP (MPa)	$1/T$ (/s)
2.77	1.3
3.34	1.7
3.92	2.1
4.95	2.5

The plastic hardening model of metal thin wall tube under pulsating hydraulic loading condition, non-pulsating hydraulic loading condition, and uniaxial tension are obtained by polynomial fitting, as shown in Eqs. (28)-(30):

$$\sigma = 562941\varepsilon^5 - 764492\varepsilon^4 + 395539\varepsilon^3 - 95471\varepsilon^2 + 11864\varepsilon + 13.657 \quad (28)$$

$$\sigma = 626233\varepsilon^5 - 821306\varepsilon^4 + 401090\varepsilon^3 - 92902\varepsilon^2 + 12045\varepsilon\text{-}37.73 \quad (29)$$

$$\sigma = 1349.2\varepsilon^{0.2876}. \quad (30)$$

3. Precision verification of tube plastic hardening model under pulsating hydraulic loading

The finite element model of tube hydroforming is established at first, and the plastic hardening model is put between the tube under pulsating and non-pulsating hydroforming conditions. Moreover, the plastic hardening model obtained by uniaxial tensile test is used as the material parameter of finite element simulation. The instantaneous tube wall thickness, maximum bulging height and axial contour of the tube middle section obtained by simulation and bulging test are compared to verify the accuracy of the model.

3.1 Establishment of finite element model

Table 1 shows the geometrical parameters and material property parameters of the tube SS304, the imported plastic hardening models are shown in Fig. 5, and the established finite element model is shown in Fig. 6. In each group, the material parameters, loading modes and boundary conditions are set in accordance with those in the hydraulic bulging test. The main contents of finite element simulation are as follows: (1) the plastic hardening model of tube based on pulsating hydroforming test is imported into the FE software to simulate the process of tube pulsating hydroforming; (2) the plastic hardening model of tube based on non-pulsating hydroforming test is imported into the FE software to simulate the process of non-pulsating tube hydroforming; (3) the plastic hardening model of tube obtained by uniaxial tensile test is imported into the FE software to simulate the non-pulsating tube hydroforming.

The main steps of FE analysis are as follows. Firstly, according to the research object, 3D modeling software is used to construct the surface model of tube hydroforming, as illustrated

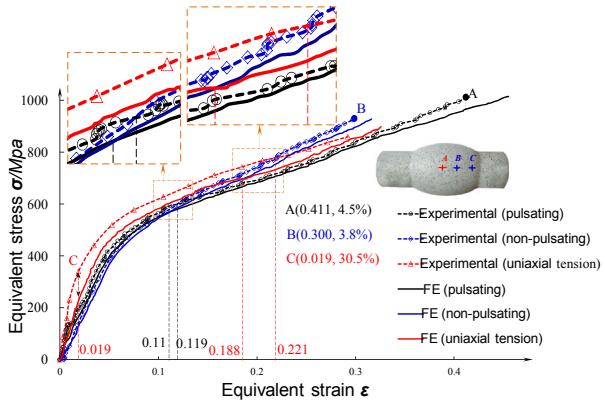

Fig. 5. The imported plastic hardening models.

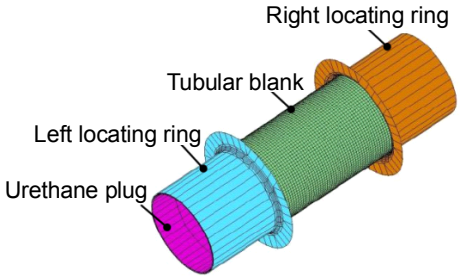

(a) FE model

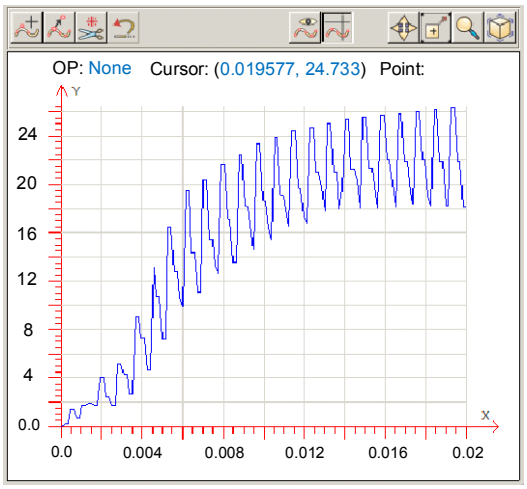

(b) Loading curve

Fig. 6. The surface model of tube hydroforming.

in Fig. 6. The geometrical parameters of the tube are the same as those of Sec. 2.4. Secondly, the surface model of tube hydroforming is imported into the DYNAFORM preprocessor software and meshed. Subsequently, the material model in the material library is used to define the material properties of deforming material. After setting the loading conditions, the result file generated by the post-processor is opened. Eventually, the calculated results are obtained.

In order to simplify the calculation, the locating ring and the urethane plug at both tube ends are set as rigid bodies, and

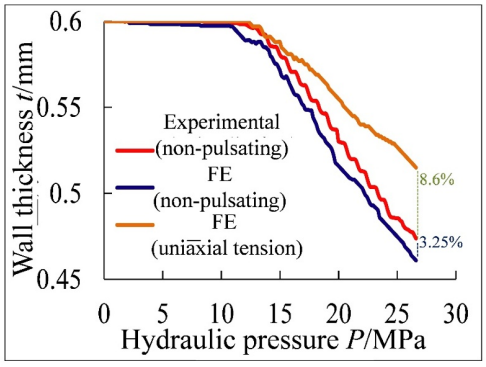

(a) Non-pulsating hydraulic loading and uniaxial tension

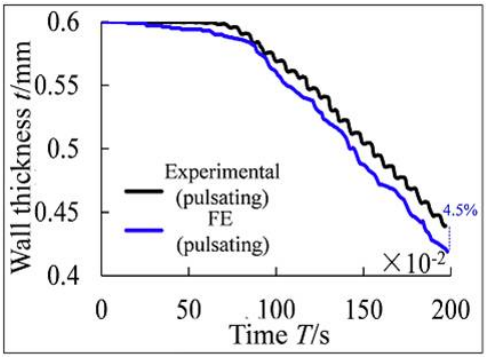

(b) Pulsating hydraulic loading

Fig. 7. The comparison between simulation value and experimental result of the tube wall thickness.

the distance between them is exactly the wall thickness of the initial tube, so as to achieve a zero clearance fit between the tube and the locating ring. Rectangular unit bodies of no more than 15 mm are divided on these rigid faces, and the same parts are divided into the same number of grids in the tube forming mold, the total number of elements is 26556.

3.2 Analysis of accuracy verification results of tube plastic hardening model

The tube wall thickness and maximum bulging height of the middle section obtained by FE simulation are compared with the bulging test results respectively, so as to verify the precision of the plastic hardening relationship of the tube under the condition of non-pulsating and pulsating hydroforming determined in this study.

The simulation values of the tube wall thickness of the middle section are compared with the bulging test value, as illustrated in Fig. 7.

As can be seen from Fig. 7, in terms of the relative error between the wall thickness of the middle section and the experimental value, the tube plastic hardening relationship of non-pulsating hydroforming obtained by the method proposed in this study is the smallest, within the range of -3.25 %. However, in terms of the relative error of the wall thickness of the middle section, the tube plastic hardening relationship obtained by

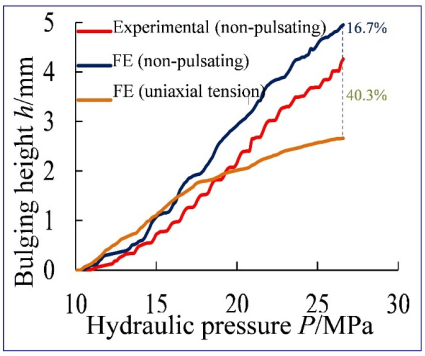

(a) Non-pulsating hydraulic loading and uniaxial tension

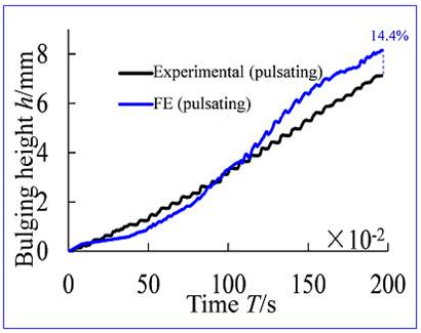

(b) Pulsating hydraulic loading

Fig. 8. The comparison between simulation value and experimental result of the maximum bulging height.

uniaxial tensile test method is the largest, which is within the range of +8.6 %.

The wall thickness of the middle cross section obtained by simulating the tube plastic hardening relationship under pulsating hydroforming determined by the method proposed in this study, within the relative error range of -4.5 %, is lower than the the corresponding value obtained in the test. Therefore, the precision of the plastic hardening relation of the tube constructed by the method proposed in this study is more accurate.

The simulation values of the maximum bulging height of the middle section of the tube are compared with the bulging test values as illustrated in Fig. 8.

As can be seen from Fig. 8, the relative error of the plastic hardening model adopted in this study between the bulging height of the middle section and the experimental result is within 16.7 %. However, the relative error of bulging height in the middle section of the tube obtained from the uniaxial tensile test is obviously larger, which is within the range of -40.3 %. The bulging height of the middle cross section under pulsating hydroforming is within 14.4 %, which is lower than the corresponding value obtained in the test. Furthermore, it is also lower than the bulging height deviation obtained by simulation in non-pulsating hydroforming.

The reasons for the discrepancies between experiment and numerical analysis are varied. The most important one is in the process of tube pulsating hydroforming, the hydraulic pressure changes cyclically according to a certain amplitude and frequency, and the same hydraulic pressure may correspond to several different wall thicknesses and maximum bulging height. So in order to make better use of the plastic hardening model and reduce the influence of fluctuations, the wall thickness and maximum bulging height at the tube neutral layer under the same bulging time is generally used as the benchmark to compare the experimental value and the simulated value.

4. Conclusions

According to the stress condition of the tube hydroforming, the axial and circumferential stress calculation formula were derived. Combined with the theory of plasticity increment, the tube equivalent strain calculation formula was obtained. According to the work principle of plastic deformation, the tube equivalent stress calculation formula was obtained. The tube plastic hardening model was obtained through curve fitting technique with experimental data. The main characteristic of this method is that it not only avoids the assumption of the bulging contour shape of the tube, but also does not need to use special equipment to directly measure the bulging contour of the tube, and the plastic hardening model obtained in this paper was more accurate. By comparing the instantaneous wall thickness and maximum bulging height of the middle section of the tube obtained by simulation and test, the precision of the tube plasticity hardening model determined under the condition of pulsating hydroforming in this study was verified.

Acknowledgments

This work was supported by National Natural Science Foundation of China (51665018) and Youth Scientific Research Project of JXEDU (GJJ171265).

Nomenclature

P (Mpa)	: Pulsating fluid pressure (Fig. 1)
T (s^{-1})	: Pulsation cycle (Fig. 1)
L (mm)	: Length of metal thin-walled tube (Fig. 2(a); Eq. (3); Table 1)
l (mm)	: Length of tube bulging area (Fig. 2(a); Eq. (3); Table 1)
i (s)	: Time i in the process of tube bulging (Fig. 2(a))
h_i (mm)	: Tube bulging height at time i (Fig. 2(a))
P_i (Mpa)	: Instantaneous internal pressure (Fig. 2(a))
r_0 (mm)	: Initial radius of thin-walled tube (Fig. 2(a); Eq. (3); Table 1)
t_0 (mm)	: Initial wall thickness of thin-walled tube (Fig. 2(a); Table 1)
σ_{az} (Mpa)	: Axial stress at point a (Fig. 2(b); Eqs. (7), (10), (11) and (14)-(16))
σ_{bz} (Mpa)	: Axial stress at point b (Fig. 2(b); Eqs. (7), (10), (11) and (14)-(16))
ρ_{az} (mm)	: Axial radius of curvature at point a (Fig. 2(b); Eq. (15))

ρ_{bz} (mm) : Axial radius of curvature at point b (Fig. 2(b); Eq. (15))
$\rho_{a\theta}$ (mm) : Circumferential radius of curvature at point a (Fig. 2(b); Eqs. (14)-(16))
$\rho_{b\theta}$ (mm) : Circumferential radius of curvature at point a (Fig. 2(b); Eqs. (14)-(16))
t_a (mm) : Wall thickness of thin-walled tube at point a (Fig. 2(b); Eqs. (7), (8), (10)-(12) and (17))
t_b (mm) : Wall thickness of thin-walled tube at point b (Fig. 2(b); Eqs. (7), (10)-(12) and (17))
t_p (mm) : Wall thickness of thin-walled tube under hydraulic pressure P (Fig. 2(b); Eqs. (7), (12), (17), (20) and (21))
dl_a (mm) : The length of the circumferential arc belong to the circle passing point a before and after bulging (Fig. 2(b); Eqs. (7), (8) and (18))
dl_b (mm) : The length of the circumferential arc belong to the circle passing point b before and after bulging (Fig. 2(b); Eqs. (7)-(9) and (18))
$d_{forming}$ (mm) : The length of the tube bulging profile from point a to point b (Fig. 2(b); Eqs. (7), (10), (11) and (13))
θ (°) : The angle between the section of the unit body and the tube axis (Fig. 2(b); Eqs. (7), (10) and (11))
φ (°) : The angle between the straight line passing through point a and b and the horizontal coordinate axis (Fig. 2(b); Eq. (19))
o_a (—) : Center of curvature at point a (Fig. 2(b))
o_b (—) : Center of curvature at point b (Fig. 2(b))
σ_θ (Mpa) : Circumferential stress (Fig. 2(c); Eqs. (20) and (21))
ψ_a (°) : The angle between the tangent of point a on the bulging profile and the horizontal coordinate axis (Fig. 2(d); Eqs. (7), (10) and (11))
ψ_b (°) : The angle between the tangent of point b on the bulging profile and the horizontal coordinate axis (Fig. 2(d); Eqs. (7), (10) and (11))
γ (°) : The angle between the line connecting point a and point b on the bulging profile and the horizontal coordinate axis (Fig. 2(d); Eqs. (7), (10) and (11))
$\sigma_{z(i)}$ (Mpa) : Axial stress at the bulging time i (Eqs. (1), (2), (20) and (21))
$\rho_{\theta(i)}$ (mm) : Circumferential radius of curvature at the bulging time i (Eqs. (1), (2), (20) and (21))
t_i (mm) : Tube wall thickness at the bulging time i (Eqs. (1) and (2))
F_f (N) : Friction between thin-walled tube and mold (Eqs. (1)-(3))
ψ_i (°) : The angle between the tangent of a point on the bulging profile and the horizontal coordinate axis (Eqs. (4), (5) and (19))
$f_{(z)}$ (—) : Bulging profile curve function (Eqs. (5) and (6))
ρ_z (mm) : Radius of axial curvature (Eqs. (6), (20) and (21))
$\varepsilon_{z(i)}$ (—) : Axial strain at any bulging time i (Eqs. (22) and (23))
$\varepsilon_{\theta(i)}$ (—) : Circumferential strain at any bulging time i (Eqs. (22) and (23))
$\varepsilon_{t(i)}$ (—) : Thickness strain at any bulging time i (Eqs. (22) and (23))
$d\varepsilon_{z(i)}$ ():(—) : The axial strain increment of tube at any bulging time i (Eqs. (23), (24) and (26))
$d\varepsilon_{\theta(i)}$ (—) : The circumferential strain increment of tube at any bulging time i (Eqs. (23), (24) and (26))
$d\varepsilon_{t(i)}$ (—) : The thickness strain increment of tube at any bulging time i (Eqs. (23), (24) and (26))
$d\varepsilon_{e(i)}$ (—) : The equivalent strain increment of tube at any bulging time i (Eqs. (24)-(26))
$\varepsilon_{e(i)}$ (—) : The equivalent strain of tube at any bulging time i (Eqs. (25)-(27))
$\sigma_{e(i)}$ (Mpa) : Equivalent stress of tube material at any bulging time i (Eqs. (26) and (27))
$\sigma_{z(i)}$ (Mpa) : Axial stress of bulging tube at any bulging time i (Eqs. (26) and (27))
$\sigma_{\theta(i)}$ (Mpa) : Circumferential stress of bulging tube at any bulging time i (Eqs. (26) and (27))
$\sigma_{t(i)}$ (Mpa) : Thickness stress of bulging tube at any bulging time i (Eqs. (26) and (27))
$\lambda_0, \lambda_1, \ldots$ (—) : The coefficients in the plastic hardening model of metal thin-walled tube (Eq. (27))
σ_b (Mpa) : Tensile strength (Table 1)
σ_s (Mpa) : Yield strength (Table 1)
K(—) : The strength coefficient (Table 1)

References

[1] K. Mori et al., Mechanism of improvement of formability in pulsating hydroforming of tubes, *International Journal of Machine Tools & Manufacture*, 47 (6) (2007) 978-984.
[2] M. Loh-Mousavi et al., 3-D finite element simulation of pulsating free bulge hydroforming of tubes, *Iranian Journal of Science & Technology*, 32 (6) (2008) 611-618.
[3] M. Zhan et al., A method for establishing the plastic constitutive relationship of the weld bead and heat-affected zone of welded tubes based on the rule of mixtures and a microhardness test, *Materials Science and Engineering*, 527 (2010) 2864-2874.
[4] P. V. Badiger et al., Cutting forces, surface roughness and tool wear quality assessment using ANN and PSO approach during machining of MDN431 with TiN/AlN-coated cutting tool, *Arabian Journal for Science and Engineering*, 44 (9) (2019) 7465-7477.
[5] P. V. Badiger et al., Effect of cutting parameters on tool wear, cutting force and surface roughness in machining of MDN431 alloy using Al and Fe coated tools, *Materials Research Express*, 6 (1) (2018) 016401.
[6] P. V. Badiger et al., Tribological behaviour of monolayer and multilayer Ti-based thin solid films deposited on alloy steel, *Materials Research Express*, 6 (2) (2018) 026419.
[7] J. W. Liu et al., Determination of flow stress of thin-walled tube based on digital speckle correlation method for hydroforming applications, *International Journal of Advanced Manufacturing Technology*, 69 (2013) 439-450.
[8] N. H. Wang et al., Comparison of constitutive relationships of

tubular materials based on incremental theory and total strain theory, *Materials Research Innovations*, 19 (2015) 710-715.
[9] Y. Lin et al., Complex stress-strain relations of tubular materials studied with a flexible hydroforming system, *Journal of Testing and Evaluation*, 45 (4) (2017) 1130-1138.
[10] J. Liu et al., A new hybrid identification method for determining the material parameters of thin-walled tube under compressive stress state, *Materials and Design*, 44 (2013) 49-58.
[11] O. Pantale et al., Influence of the constitutive flow law in FEM simulation of the radial forging process, *Journal of Engineering* (2013) 1-8.
[12] Z. Temim et al., Experimental characterization and inverse constitutive parameters identification of tubular materials for tube hydroforming process, *Materials and Design*, 49 (2013) 866-877.
[13] N. Boudeau et al., A simplified analytical model for post-processing experimental results from tube bulging test: theory, experimentations, simulations, *International Journal of Mechanical Sciences*, 65 (2013) 1-11.
[14] Z. H. Tao et al., Optimization method of loading path for tube hydroforming, *Applied Mechanics and Material*, 109 (2012) 676-680.

Guolin Hu is a Ph.D. candidate of the School of Mechanical and Electrical Engineering, Jiangxi University of Science and Technology, Ganzhou, China. He received his master degree in Mechanical Manufacture and Automation from Guilin University of Electronic Technology. His research interests include machine manufacturing, metal forming and electromechanical control.

Chunrong Pan is a Professor of the School of Mechanical and Electrical Engineering, Jiangxi University of Science and Technology, Ganzhou, China. He received his Ph.D. degree in Mechanical Manufacture and Automation from Guangdong University of Technology. His research interests include machine manufacturing, optimization algorithm and electromechanical control.